

The Host Galaxies of Narrow-Line Seyfert 1s: Evidence for Bar-Driven Fueling

D. M. Crenshaw¹, S. B. Kraemer², & J.R. Gabel²

ABSTRACT

We present a study of the host-galaxy morphologies of narrow- and broad-line Seyfert 1 galaxies (NLS1s and BLS1s) based on broad-band optical images from the *Hubble Space Telescope* archives. We find that large-scale stellar bars, starting at ~ 1 kpc from the nucleus, are much more common in NLS1s than BLS1s. Furthermore, the fraction of NLS1 spirals that have bars increases with decreasing full-width at half-maximum (FWHM) of the broad component of $H\beta$. These results suggest a link between the large-scale bars, which can support high fueling rates to the inner kpc, and the high mass-accretion rates associated with the supermassive black holes in NLS1s.

Subject headings: galaxies: Seyfert

1. Introduction

Seyfert galaxies are relatively nearby ($z \lesssim 0.1$), moderate-luminosity ($L_{bol} = 10^{43} - 10^{45}$ erg s⁻¹) active galaxies. The large-scale morphologies of these galaxies typically resemble those of normal (i.e., inactive) spiral galaxies, although there are some examples of peculiar or interacting systems (De Robertis, Hayhoe, & Yee 1998). Optical and UV spectra of their nuclei are characterized by strong atomic emission lines. Based on the widths of these lines, Seyfert galaxies are generally divided into two types (Khachikian & Weedman 1974): Type 1s possess broad permitted lines with full-width at half-maximum (FWHM) typically > 1000 km s⁻¹ and narrow forbidden lines with FWHM $\lesssim 500$ km s⁻¹, while the spectra of Type 2s show narrow permitted and forbidden lines. Those Seyferts that show both broad and narrow components in their permitted lines are classified as intermediate types, ranging from 1.2 to 1.9 (Osterbrock, 1977; 1981).

¹Department of Physics and Astronomy, Georgia State University, Atlanta, GA 30303; crenshaw@chara.gsu.edu

²Catholic University of America, and Laboratory for Astronomy and Solar Physics, NASA's Goddard Space Flight Center, Code 681, Greenbelt, MD 20771; stiskraemer@yancey.gsfc.nasa.gov.

Osterbrock & Pogge (1985) discovered a class of active galactic nuclei (AGN) with relatively narrow ($\text{FWHM} < 2000 \text{ km s}^{-1}$) permitted lines, like Seyfert 2 galaxies, but with emission-ratios that indicate the presence of a high-density region, like the broad-line region (BLR) in Seyfert 1 galaxies. They dubbed these objects “Narrow-Line Seyfert 1s” (NLS1s). As discussed by Mathur (2000a, 2000b), NLS1s possess a number of interesting spectral properties. They show strong Fe II and weak [O III] $\lambda 5007$ emission relative to $\text{H}\beta$, which puts them at one extreme of eigenvector 1 of Boroson & Green (1992), which was determined from principal component analysis of a large sample of low-redshift quasars and Seyfert galaxies. Compared to broad-line Seyfert 1s (BLS1s), the X-ray continua of NLS1s are characterized by steep slopes and rapid variability, particularly in the soft ($\leq 1 \text{ keV}$) band (Boller, Brandt, & Fink 1996; Brandt, Mathur, & Elvis 1997). Wills et al. (1999) found unusually high N V $\lambda 1240$ / C IV $\lambda 1550$ flux ratios in NLS1s, which may be indicative of high nitrogen abundances, as would result from metal enrichment due to a recent burst of star formation (see also Shemmer & Netzer 2002). The mid-IR brightness of a number of NLS1s provides further evidence of recent or current star formation (Moran, Halpern, & Helfand 1996).

There are several models to explain the unusual properties of NLS1s, and in particular the narrowness of their line profiles. Wandel & Peterson (1999) suggested that the BLRs may be relatively farther away from the central continuum source in NLS1s, due to over-ionization of the gas close to the active nucleus. However, based on estimates of the BLR sizes from reverberation mapping, Peterson et al. (2000) argue this cannot generally be the case. Another possibility is that the BLR is flattened and viewed roughly face-on, with narrow line profiles as a result, although Peterson et al. found no compelling evidence for such a preferred viewing angle unless the narrow emission-line regions are mis-aligned with the accretion-disk/black hole systems in these objects.

The current widely-accepted paradigm is that, while AGN in general are powered by accretion of material onto a supermassive central black hole, NLS1s possess black holes of relatively modest mass ($\leq 10^7 M_{\odot}$), that are accreting matter at or above their Eddington limits (Pounds, Done, & Osborne 1995). This view is supported by recent observational results that indicate that NLS1s possess significantly smaller black-hole mass to bulge mass ratios than their broad-line counterparts (Mathur, Kuraszkiwicz, & Czerny 2001; Wandel 2002). In this scenario, the narrow line widths are simply due to clouds in motion around the small-mass black hole, while the steep soft X-ray continuum is the high-energy tail of the “Big Blue Bump”, which is presumably emission from the accretion disk that peaks in the extreme ultraviolet (EUV). NLS1s could therefore be analogous to the “strong soft” states of galactic black holes at high accretion rates (Pounds et al. 1995). Due to the high accretion rates, the disks in NLS1s are likely much hotter than those in BLS1s, and hence

the emission is peaked at higher energies. Wang & Netzer (2003) showed that high-accretion rates result in an extremely thin disk which emits a double-peaked continuum, with a peak in the EUV/soft X-ray due to the disk itself, and a high energy peak due to a hot corona. Based on this model, they suggest that most of the 54 NLS1s in the Véron-Cetty, Véron, & Gonçalves (2001) sample are super-Eddington accretors. Assuming that NLS1s are high-rate accretors, and considering the other evidence of extreme activity, Mathur (2000a, 2000b) suggested that NLS1s are in an early phase of activity and may be the low-redshift analogs of high- z QSOs (however, see Constantin & Shields 2003).

In order to fuel Seyfert galaxies and other AGN, material must be transported from the host galaxy into the inner nucleus, requiring some means by which the material loses angular momentum. One possibility is interactions or mergers with other nearby galaxies (Toomre & Toomre 1972; Adams 1977). However recent studies indicate that Seyfert galaxies do not have more close companions than do normal galaxies, and, furthermore, a substantial fraction of Seyfert galaxies show no evidence for recent mergers (De Robertis, Yee, & Hayhoe 1998, and references therein).

Another process for fueling AGN that has received considerable attention is gas inflow along a stellar bar (Simkin, Su, & Schwarz 1980). Theoretical studies show that the gas can lose its angular momentum after encountering the gravitational potential of a bar and be transported inward (Shlosman, Begelman, & Frank 1989). However, most observational studies in this area have found similar fractions of bars for Seyferts and normal galaxies (Heckman 1980; Simkin et al. 1980; Ho, Filippenko, & Sargent 1997; Mulchaey, Regan, & Kundu 1997; Mulchaey & Regan 1997), although Knappen, Shlosman, & Peletier (2000) found a slightly higher percentage of IR bars in Seyferts (80%) compared to normal galaxies (60%). Interestingly, the percentages of Seyfert or normal galaxies that have bars vary substantially among these studies, from $\sim 30\%$ to $\sim 80\%$. These discrepancies are probably due to the sample selection (e.g., luminous vs. average spirals), wave band (IR observations tend to reveal more bars than optical images, Mulchaey & Regan 1997), and identification criteria (e.g., whether or not to include weak bars). Nevertheless, well-defined samples that use consistent criteria nearly always find equal percentages of bars in Seyfert and normal galaxies (with the exception noted above). Since there is strong evidence that most normal galaxies contain inactive supermassive black holes (Kormendy & Richstone 1995), the above finding indicates that while bars may be important for driving gas into the inner regions, there are other factors that contribute to the presence of nuclear activity.

Dynamical models indicate that a bar potential can drive material to within ~ 1 kpc from the AGN, at which point the transport will be halted at the Inner Lindblad Resonance and the infalling gas will form a disk (Shlosman, et al. 1989). If global nonaxisymmetrical

instabilities are present, a secondary, gaseous bar can develop at small distances from the nucleus ($\lesssim 1$ kpc), and provide a means to drive the gas in towards the active nucleus (Shlosman, et al. 1989; Heller & Shlosman 1994). In fact, Maiolino et al. (2000) found evidence for gas motion along a secondary bar in the nucleus of the Seyfert 2 Circinus Galaxy. However, it appears that secondary gas bars are fairly rare among Seyfert galaxies. The most efficient way to detect these bars is through the extinction or reddening caused by their embedded dust. *Hubble Space Telescope* (*HST*) IR and optical images indicate that only 10 – 20% of Seyfert galaxies show nuclear (at distances $\lesssim 1$ kpc from the nucleus) dust bars (Regan & Mulchaey 1999; Martini & Pogge 1999; Pogge & Martini 2002). Instead, the *HST* images reveal that most ($\sim 80\%$) Seyfert galaxies show nuclear dust spirals (Regan & Mulchaey 1999; Pogge & Martini 2002; Martini et al. 2003). Although these structures are common to both barred and unbarred Seyferts, all of the “grand design” nuclear spirals (so-called by their resemblance to the large scale spiral structure of the same name) are found in barred galaxies (Martini et al. 2003). The grand design spirals appear to connect to dust lanes on the leading edge of the large-scale stellar bars, suggesting a connection to shock fronts in the bars. However, Martini et al. (2003) find that dust spirals in Seyfert galaxies are not statistically more numerous than those in normal galaxies. Thus, it is unclear exactly how the dust spirals fuel the AGN and what mechanism(s) actually control the onset of nuclear activity.

If the high accretion-rate paradigm for NLS1s is correct, it suggests that the fueling of the AGN is more efficient in these Seyferts than in their BLS1 counterparts. If so, perhaps there is a connection between large-scale properties and the high accretion rates in NLS1s. Krongold, Dultzin-Hacyan, and Marziani (2001) examined host galaxies and environments, and found no statistical difference between the frequency of companion galaxies in NLS1s and BLS1s. Another possibility is a difference in their large-scale morphologies. In this paper, we provide evidence that, stellar bars are much more common in NLS1s than BLS1s. These large-scale bars, which typically begin at ~ 1 kpc from the nucleus and extend to 5 – 10 kpc, represent an efficient means for transporting large amounts of gas to the inner regions, which can presumably support the high accretion rates in the nuclei of NLS1s.

2. Sample and Analysis

Our sample contains primarily the *HST* broad-band images of Seyfert 1 galaxies obtained by Malkan, Gorjian, & Tam (1998). This is a uniform sample of 91 Seyfert 1 galaxies at $z \leq 0.035$ observed with the Wide Field Planetary Camera 2 (WFPC2) through the F606W filter (centered near 6000 Å). Single exposures of duration 500 s were obtained with nearly all the

Seyfert nuclei located on the planetary camera (PC) chip, yielding a spatial resolution of $0''.1$. The number of NLS1s in this sample is small (13); to increase that number, we searched the *HST* archives for NLS1s in the Véron-Cetty et al. (2001) sample that have WFPC2 broad-band optical images. We found 6 additional NLS1s, which extend to higher redshifts (up to $z = 0.084$); the effects of including them to make a larger, more heterogeneous sample (in terms of redshift) will be discussed.

We retrieved all of the WFPC2 images from the *HST* archives, to display a larger field of view ($37'' \times 37''$, the projected size of the PC) than the images published (mostly $9'' \times 9''$) in Malkan et al. (1998). The Malkan et al. sample consists of single images of each Seyfert galaxy, and we removed only point-like cosmic-ray hits using automated routines. The remaining galaxies had multiple images, and we removed both point-like and glancing hits through intercomparison of the images. In practice, residual or remaining cosmic ray hits, saturation of the nuclei, or other defects were easily recognized in these images and had little effect on our assessment of the large-scale morphology of the host galaxies.

To ensure objectivity, we scrambled the order of the *HST* images and the three coauthors independently classified their morphologies without knowledge of Seyfert 1 subclass (NLS1 or BLS1) or the name of the galaxy. We classified the galaxies into one of 6 major groups: S (spiral), SB (spiral with a noticeable bar), E (elliptical), I (irregular), P (point-source, only the active nucleus is visible), or ? (uncertain) (note that we did not attempt to assign Hubble subclasses). For each galaxy, at least two of the three independent classifications agreed (in most cases all three agreed), and we adopted the majority view.

A large majority of the galaxies in the sample are at redshifts $z = 0.01 - 0.035$, which yield projected distances of $7 - 25$ kpc across the PC for $H_0 = 75 \text{ km s}^{-1} \text{ Mpc}^{-1}$. In the Malkan sample, there are 11 out of 91 galaxies at smaller redshifts, extending down to $z = 0.002$ (1.4 kpc across the PC). For these galaxies in particular, we also examined the full WFPC2 images to assess their large-scale morphologies (each WF chip has a field of view of $1'.3 \times 1'.3$). The six additional galaxies from Véron-Cetty et al. (2001) have redshifts up to 0.084, corresponding to 60 kpc across the PC.

In Table 1, we give the results of our classifications. The galaxies are first listed in the same order as in Malkan et al. (1998), and are followed by the six additional NLS1 galaxies from Véron-Cetty et al. (2001). We also list the redshifts, our morphological classifications (“CKG”), and those based on the same images from Malkan et al. (“MGT”), which include Hubble subclasses. The classes of Seyfert nuclei (BLS1 or NLS1) are based on the listings in the catalog of Véron-Cetty & Véron (2001); the BLS1s include Seyferts from types 1 to 1.9. In the last two columns, we give measurements of the full-width at half-maximum (FWHM) of the broad component of $H\beta$ (or in a few cases, $H\alpha$), and the references that

these measurements were obtained from. Note that 35 Seyfert galaxies in the sample have previously been classified as NLS1s or BLS1s on the basis of their optical spectra, but measurements of the FWHMs of the broad lines have not been published.

We note that our general morphological classes agree well with those of Malkan et al. Of the 91 galaxies, there are only 11 discrepancies, and of the 74 galaxies that we both identified as spirals, there is disagreement on the presence or absence of a bar in only 6 galaxies (5 BLS1s, 1 NLS1). To illustrate our classifications, we show the *HST* images of the NLS1s in our sample in Figures 1 and 2. NGC 4051 is not shown, since at its very low redshift ($z = 0.0023$) the PC only spans 1.6×1.6 kpc. Examination of the Palomar Sky Survey and other ground-based images (Tully et al. 1996) shows a strong bar that can be seen extending into the larger WFPC2 frame.

3. Results

We consider the 92 Seyfert galaxies in Table 1 with definite morphological classifications (i.e., ignoring the “P” and “?” classes). From this group, we have classified 91% as spirals, and of the spirals, we have classified 33% of the spirals as barred. The latter is consistent with percentages from studies that have identified strong bars in optical images of both active and normal spiral galaxies (Mulchaey et al. 1997; Malkan et al. 1998; see also §1).

However, it is obvious from Table 1 that most of the NLS1 galaxies are barred spirals, and most of the BLS1 galaxies are normal spirals. Quantitatively, if we consider the 84 spirals in this sample, then 65% (11/17) of the NLS1 spirals have bars, whereas only 25% (17/67) of the BLS1 spirals have bars. If we consider only the Malkan et al. sample, then 64% (7/11) of the NLS1 spirals have bars, which is essentially identical to the result for the full sample. If we use Malkan et al.’s (1998) classifications, then 30% (20/67) of the BLS1 spirals show bars and 55% (6/11) of the NLS1 spirals show bars.

To further characterize the trend of bars in NLS1 galaxies, Figure 3 shows histograms of the fraction of spirals that have bars as a function of the FWHM ($H\beta$) on a log scale. The shaded regions show a clear trend of decreasing fraction of bars with increasing FWHM for the entire sample. The trend continues through the three bins associated with NLS1s ($\text{FWHM} < 2000 \text{ km s}^{-1}$) to the first bin for the BLS1s. The fraction levels out thereafter, and is essentially constant for all BLS1s regardless of FWHM. Interestingly, the four NLS1 spirals in the full sample with the smallest FWHM ($600 - 1000 \text{ km s}^{-1}$) all show bars.

The hatched region in Figure 3 shows that the same trend occurs for the more uniform Malkan et al. subsample; there is only a slightly lower fraction of bars in NLS1s with widths

in the range $1000 - 2000 \text{ km s}^{-1}$ compared to the full sample. It is clear from Table 1 that the number of NLS1s in each bin is quite small (as low as 3) for this subsample, and a larger, more uniform sample of images for both BLS1s and NLS1s would be helpful for testing this trend.

4. Discussion

Our analysis of *HST*/WFPC2 images reveals that stellar bars are more common in NLS1s, particularly those with very narrow $H\beta$ profiles, compared to BLS1s. This suggests a link between the high fueling rates that can be provided by the bars and the high accretion rates commonly associated with NLS1s. These large-scale stellar bars often extend down to 1 kpc from the nuclei of these galaxies. Inside a radius of ~ 1 kpc, nuclear dust spirals, and in a few cases dust bars, are likely to be directly responsible for transporting fuel to the active nucleus. However, the exact connection between large-scale bars, inner dust spirals and bars, and accretion rates in the nucleus is unclear. We outline one possible scenario below.

Based on a variety of evidence, it has been suggested that NLS1s are in an early stage of activity (Mathur 2000a, 2000b). If so, the presence of bars suggests the following evolutionary sequence for galaxies that become active. 1) Initially, the galaxy is a normal spiral, albeit with a small black hole mass M_{BH} ($< 10^7 M_{\odot}$). Although studies of nearby inactive galaxies find few with M_{BH} this small (Magorrian et al. 1998; Merritt & Ferrarese 2001; Kormendy & Gebhardt 2001), Wandel (2002) suggested that the sample derived from stellar dynamics is biased towards detecting higher mass M_{BH} , since detecting smaller mass sources requires higher spatial resolution, which is only possible in the most nearby galaxies. Hence there may be a large, undetected population of small M_{BH} in inactive galaxies. 2) Due to either a tidal disruption or simply an asymmetrical distribution of mass in the inner disk of the galaxy, a stellar bar forms within a few $\times 10^8$ yrs (Combes & Elmegreen 1993). The presence of a bar can efficiently drive gas into the inner nucleus (Friedli & Benz 1993), which can be detected in the form of inner dust spirals or bars. 3) At this point, the galaxy starts the NLS1 phase, powered by a small central black hole accreting at close to its Eddington limit. Within 10^8 yrs, the bar can trigger star formation (Hunt & Malkan 1999, and references therein), which suggests that the evidence for active star formation in NLS1s may also be related to the presence of a bar. Dynamical models indicate that once $\sim 5\%$ of the mass of the disk is redistributed into the inner nucleus, the bar will be destroyed (Friedli & Benz 1993; Norman et al. 1996). Although models predict that this will take a few $\times 10^9$ yrs, they do not typically include the effects of asymmetrical mass distribution in the inner nucleus,

which may shorten the lifetime of the bar (Norman et al. 1996). 4) At this stage, M_{BH} will have increased sufficiently (several to ten times its initial mass) such that the galaxy appears as a BLS1. Since BLS1s are substantially sub-Eddington, the fueling rate must also have decreased significantly. There are a number of possible explanations for this, including the weakening of the bar, the diminished reserve of fuel in the inner disk, or the effect of the energized AGN itself, which can drive mass outflow (see Crenshaw, Kraemer, & George 2003). Interestingly, Hunt & Malkan (1999) find evidence that Seyferts show outer stellar rings more often than inactive galaxies. Outer rings take \sim several $\times 10^9$ yrs to form, and are likely to outlast the stellar bars. Hence, the rings may be a remnant of the earlier, bar-driven phase of what are now BLS1s.

Testing the above scenario, and determining the physical connection between large-scale bars and fueling of active nuclei, could be accomplished with more extensive *HST* images of the nuclear regions in NLS1s. The fueling flow can be traced via deep optical and IR images of the dust lanes, and possibly narrow-band images of the low-ionization emission. Narrow-band observations of the high-ionization outflowing gas could be used to determine the geometry of infall versus outflow. Finally, UV images could be used to look for evidence of circumnuclear starbursts and explore their connection to AGN activity.

This research has made use of the NASA/IPAC Extragalactic Database (NED) which is operated by the Jet Propulsion Laboratory, California Institute of Technology, under contract with the National Aeronautics and Space Administration. This research has also made use of NASA's Astrophysics Data System Abstract Service. Some of the data presented in this paper were obtained from the Multimission Archive at the Space Telescope Science Institute (MAST). Support for MAST for non-HST data is provided by the NASA Office of Space Science via grant NAG5-7584 and by other grants and contracts.

REFERENCES

- Acosta-Pulido, J.A., Vila-Vilaro, B., Perez-Fournon, I., Wilson, A.S., & Tsvetanov, Z.I. 1996, *ApJ*, 464, 177
- Adams, T. 1977, *ApJS*, 33, 19
- Boller, T., Brandt, W.N., & Fink, H. 1996, *A&A*, 305, 53
- Boroson, T.A. & Green, R.F., 1992, *ApJS*, 80, 109
- Brandt, W.N., Mathur, S., & Elvis, M. 1997, *MNRAS*, 285, L25
- Combes, F. & Elmegreen, B.G. 1993, *A&A*, 271, 391
- Constantin, A. & Shields, J.C. 2003, *ApJ*, in press
- Crenshaw, D.M. 1986, *ApJS*, 62, 821
- Crenshaw, D.M., Kraemer, S.B., & George, I.M. 2003, *ARA&A*, in press
- De Robertis, M.M., Hayhoe, K., & Yee, H.K.C. 1998, *ApJS*, 115, 163
- De Robertis, M.M., Yee, H.K.C. & Hayhoe, K. 1998, *ApJ*, 496, 93
- Friedli, D. & Benz, W. 1993, *A&A*, 268, 65
- Ghigo, F.D., Wyckoff, S., Wardle, J.F.C., Cohen, N.L. 1982, *AJ*, 87, 1438
- Gregory S.A., Tifft W.G., & Cocke W.J. 1991, *AJ*, 102, 1977
- Halpern, J.P. & Filippenko, A.V. 1986, *AJ*, 91, 1019
- Heckman, T. M. 1980, *A&A*, 88, 365
- Heller, C.H. & Shlosman, I. 1994, *ApJ*, 424, 84
- Ho, L.C., Filippenko, A.V., & Sargent, W.L.W. 1997, *ApJ*, 487, 579
- Ho, L.C., Filippenko, A.V., Sargent, W.L.W., & Peng, C.Y. 1997, *ApJS*, 112, 391.
- Hunt, L.K., & Malkan, M.A. 1999, *ApJ*, 516, 660
- Khachikian, E.Ye. & Weedman, D.W. 1974, *ApJ*, 192, 581
- Knapen, J.H., Sholsman, I., & Peletier, R.F. 2000, *ApJ*, 529, 93
- Kollatschny, W., Bischoff, K., & Dietrich, M. 2000, *A&A*, 361, 901
- Kollatschny W. & Fricke K.J. 1983, *A&A*, 125, 276
- Kormendy, J. & Gebhardt, K. 2001, *Proc. of the 20th Texas Symp.*, ed. H. Martel & J.C. Wheeler, in press
- Kormendy, J. & Richstone, D. 1995, *ARA&A*, 33, 581

- Kriss, G.A., Hartig, G.F., Armus, L., Blair, W.P., Caganoff, S., & Dressel, L. 1991, *ApJ*, 377, 13
- Kronggold, Y., Dultzin-Hacyan, D., & Marziani, P. 2001, *AJ*, 121, 702
- Magorrian, J., et al. 1998, *AJ*, 115, 2285
- Malkan, M.A., Gorjian, V., & Tam, R. 1998, *ApJS*, 117, 25
- Maiolino, R., Alonso-Herrero, A., Anders, S., Quillen, A., Rieke, M.J., Rieke, G.H., & Tacconi-Garman, L.E. 2000, *ApJ*, 531, 219
- Martini, P. & Pogge, R.W. 1999, *AJ*, 118, 2646
- Martini, P., Regan, M.W., Mulchaey, J.S., & Pogge, R.W. 2003, *ApJ*, in press
- Marziani, P., Sulentic, J.W., Zamanov, R., Calvani, M., Dultzin-Hacyan, D., Bachev, R., & Zwitter, T. 2003, *ApJS*, 145, 199
- Mathur, S. 2000a, *MNRAS*, 314, L17
- Mathur, S. 2000b, *NewAR*, 44, 469
- Mathur, S., Kuraszkiewicz, J., Czerny, B. 2001, *NewA*, 6, 321
- Merritt, D., & Ferrarese, L. 2001, *MNRAS*, 320, L30
- Moran, E.C., Halpern, J. P., & Helfand, D.J. 1996, *ApJS*, 106, 341
- Mulchaey, J.S., & Regan, M.W. 1997, *ApJ*, 482, L135
- Mulchaey, J.S., Regan, M.W., & Kundu, A. 1997, *ApJS*, 110, 299
- Norman, C.A., Sellwood, J.A., & Hasan, H. 1996, *ApJ*, 462, 114
- Osterbrock, D.E. 1977, *ApJ*, 215, 733
- Osterbrock, D.E. 1981, *ApJ*, 249, 462
- Osterbrock, D.E., & Pogge, R.W. 1985, *ApJ*, 297, 1660
- Osterbrock, D.E. & Shuder, J.M. 1982, *ApJS*, 49, 149
- Peterson, B.M., et al. 2000, *ApJ*, 542, 161
- Pogge, R.W. & Martini, P. 2002, *ApJ*, 569, 624
- Pounds, K.A., Done, C., & Osborne, J.P. 1995, *MNRAS*, 277, L5
- Regan, M.W. & Mulchaey, J.S., 1999, *AJ*, 117, 2676
- Rodriguez-Ardila A., Pastoriza M.G., & Donzelli C.J. 2000, *ApJS*, 126, 63
- Shemmer, O. & Netzer, H. 2002, *ApJ*, 567, L19
- Shlosman, I., Begelman, M.C., & Frank, J. 1990, *Nature*, 345, 679

- Simkin, S.M., Su, H.J., & Schwarz, M.P. 1980, *ApJ*, 237, 404
- Stirpe, G.M. 1990, *A&AS*, 85, 1049
- Toomre, A. & Toomre, J. 1972, *ApJ*, 178, 623
- Tully, R.B., Verheijen, M.A.W., Pierce, M.J., Huang, J.-S., & Wainscoat, R.J. 1996, *AJ*, 112, 2471
- Véron-Cetty, M.-P. & Véron, P. 2001, *A&A*, 374, 92
- Véron-Cetty, M.-P., Véron, P., & Gonçalves, A.C. 2001, *A&A*, 372, 730
- Wandel, A. 2000, *NEWAR*, 44, 427
- Wandel, A. 2002, *ApJ*, 565, 762
- Wandel, A. & Peterson, B.M. 1999, *ApJ*, 526, 579
- Wang, J.-M., & Netzer, H. 2003, *A&A*, 398, 927
- Wills, B.J., Laor, A., Brotherton, M.S., Wills, D., Wilkes, B.J., Ferland, G.J., & Shang, Z. 1999, *ApJ*, 515, L53
- Winkler, H. 1992, *MNRAS*, 257, 677

Fig. 1.— *HST* WFPC2 (PC) images of NLS1s in the Malkan et al. (1998) sample. The field of view has been slightly trimmed to $34'' \times 34''$. Next to the name of each galaxy, the projected distances across the field of view are given assuming $H_0 = 75 \text{ km s}^{-1} \text{ Mpc}^{-1}$.

Fig. 2.— *HST* WFPC2 (PC) images of NLS1s from Véron-Cetty et al (2001). The field of view has been trimmed to $18''.4 \times 18''.4$ to show the large-scale structure more clearly. Next to the name of each galaxy, the projected distances across the field of view are given assuming $H_0 = 75 \text{ km s}^{-1} \text{ Mpc}^{-1}$.

Fig. 3.— Histogram showing the fraction of Seyfert spirals with bars as a function of the full-width at half-maximum (FWHM) of the broad component of the $H\beta$ emission line. The shaded region is for the full sample, whereas the hatched region is for the Malkan et al. (1998) subsample.

Table 1. Properties of Seyfert 1 Galaxies in Sample

Name	Redshift	Morph. CKG	Morph. MGT	Class	FWHM (km s ⁻¹)	Ref. ^a
ESO215-G14	0.019	S	Sa	BLS1		
ESO323-G77	0.015	S	Sa/b	BLS1	2500	W92
ESO354-G4	0.033	S	Sa	BLS1		
ESO362-G18	0.013	S	Sa	BLS1	4000	W92
ESO438-G9	0.024	SB	SBc/d	BLS1	5000	K83
F51	0.014	S	Sa	BLS1	2700	W92
F1146	0.032	S	Sb	BLS1	4300	W92
HEAO-1-0307-730	0.028	SB	S(B)a	BLS1	2900	W92
HEAO1143-181	0.033	I	I	BLS1	2400	W92
HEAO2106-098	0.027	P	P	BLS1	3835	R00
IC1816	0.017	SB	SBa/b	BLS1		
IC4218	0.019	S	Sa	BLS1		
IC4329A	0.016	S	Sa	BLS1	4800	W92
IR1319-164	0.017	S	Sb	BLS1		
IR1333-340	0.008	S	SO	BLS1	2400	W92
MCG6-26-12	0.032	SB	SB0	NLS1	1145	V01
MCG8-11-11	0.020	S	SB0	BLS1	3630	O82
MARK6	0.019	S	S0	BLS1		
MARK10	0.030	S	Sa/b	BLS1	2400	O77
MARK40	0.020	?	S0	BLS1	2000	O77
MARK42	0.024	SB	SBa	NLS1	865	V01
MARK50	0.023	S	S0	BLS1		
MARK79	0.022	SB	SBc	BLS1	4950	O82
MARK279	0.031	S	Sa	BLS1	6860	O82
MARK290	0.029	S	E	BLS1	2550	O82
MARK334	0.022	S	I	BLS1		
MARK335	0.025	P	?	NLS1	1350	O82
MARK352	0.015	E	E	BLS1	3800	O77
MARK359	0.017	SB	SBb/c	NLS1	900	V01
MARK372	0.031	S	Sa	BLS1	5500	G91
MARK382	0.034	SB	SBa	NLS1	1280	V01
MARK423	0.032	S	Sb	BLS1	9000	O81
MARK471	0.034	SB	SBc	BLS1		
MARK493	0.031	SB	S(B)a	NLS1	740	V01
MARK516	0.028	S	Sc	BLS1	4000	O81
MARK530	0.029	S	Sa	BLS1	6560	K00
MARK543	0.026	S	Sc	BLS1		

Table 1—Continued

Name	Redshift	Morph. CKG	Morph. MGT	Class	FWHM (km s ⁻¹)	Ref. ^a
MARK590	0.027	S	Sa	BLS1	2680	S90
MARK595	0.028	S	Sa	BLS1	2360	S90
MARK609	0.032	S	Sa/b	BLS1		
MARK699	0.034	E	E	NLS1	840	O81
MARK704	0.029	SB	SBa	BLS1	5500	S90
MARK744	0.010	S	Sb	BLS1		
MARK766	0.012	SB	SBc	NLS1	1630	V01
MARK817	0.033	SB	SBc	BLS1	4300	O82
MARK833	0.039	I	I	BLS1		
MARK871	0.034	S	Sb	BLS1	3690	M03
MARK885	0.026	SB	SBb	BLS1		
MARK896	0.027	S	Sc	NLS1	1135	V01
MARK915	0.025	S	Sa	BLS1		
MARK1040	0.016	S	Sb	NLS1	1830	O82
MARK1044	0.016	S	Sa	NLS1	1010	V01
MARK1126	0.010	S	Sb	BLS1		
MARK1218	0.028	SB	SBa	BLS1		
MARK1330	0.009	S	Sb/c	BLS1		
MARK1376	0.007	?	edge on	BLS1		
MARK1400	0.029	S	Sa	BLS1		
MARK1469	0.031	S	Sa	BLS1		
MS1110+2210	0.030	E	E	BLS1		
NGC235	0.022	S	Sa/b	BLS1		
NGC526A	0.018	I	E/S0	BLS1		
NGC1019	0.024	SB	SBb	BLS1		
NGC1566	0.004	S	Sb	BLS1	2580	K91
NGC2639	0.011	S	Sb	BLS1	3100	H97
NGC3227	0.003	?	?	BLS1	3920	S90
NGC3516	0.009	S	S0	BLS1	4760	C86
NGC3783	0.009	SB	I	BLS1	2980	S90
NGC4051	0.002	SB	Sb	NLS1	1120	V01
NGC4235	0.007	S	?	BLS1	7600	H97
NGC4748	0.014	S	Sa	NLS1	1565	V01
NGC5252	0.022	S	S0	BLS1	2500	A96
NGC5548	0.017	S	Sa	BLS1	5610	S90
NGC5674	0.025	SB	SBc	BLS1		
NGC5940	0.033	SB	SBc	BLS1	5240	M03

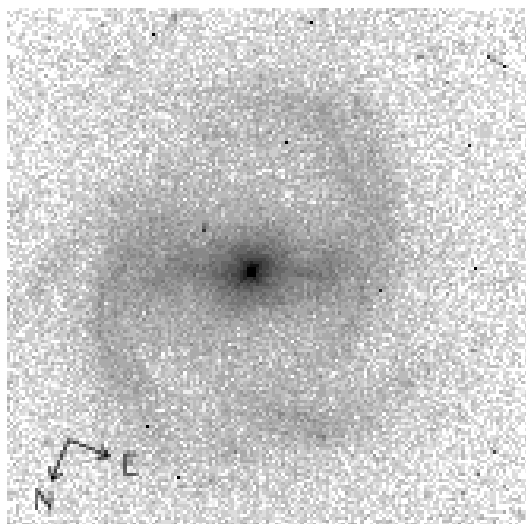
Table 1—Continued

Name	Redshift	Morph. CKG	Morph. MGT	Class	FWHM (km s ⁻¹)	Ref. ^a
NGC6104	0.028	SB	SBb	BLS1		
NGC6212	0.030	S	Sb	BLS1	6050	H86
NGC6860	0.015	S	Sb	BLS1	3900	W92
NGC7213	0.006	S	Sa	BLS1	3200	W92
NGC7314	0.006	S	Sd	BLS1		
NGC7469	0.017	S	Sb/c	BLS1	3460	C86
IIZW10	0.034	S	?	BLS1	3760	M03
PKS0518-458	0.034	E	E	BLS1	5020	M03
TOL1059+105	0.034	S	S0	BLS1		
TOL2327-027	0.033	S	SB	BLS1		
UM146	0.017	S	SBa	BLS1		
UGC3223	0.018	S	S(B)b/c	BLS1	4740	S90
WAS45	0.024	SB	Sa	BLS1		
UGC10683B	0.031	SB	SBa	BLS1		
UGC12138	0.025	SB	SBa	BLS1		
UM614	0.033	S	S0	BLS1		
X0459+034	0.016	E	E	BLS1	4320	G82
IZW1 ^b	0.061	SB	-	NLS1	1400	O77
MS0144.2-0055 ^b	0.080	S	-	NLS1	1100	V01
MARK705 ^c	0.028	SB	-	NLS1	1790	V01
MS1217.0+0700 ^b	0.080	S	-	NLS1	1765	V01
MS1519.8-0633 ^b	0.084	SB	-	NLS1	1115	V01
MS2210.2+1827 ^b	0.079	SB	-	NLS1	690	V01

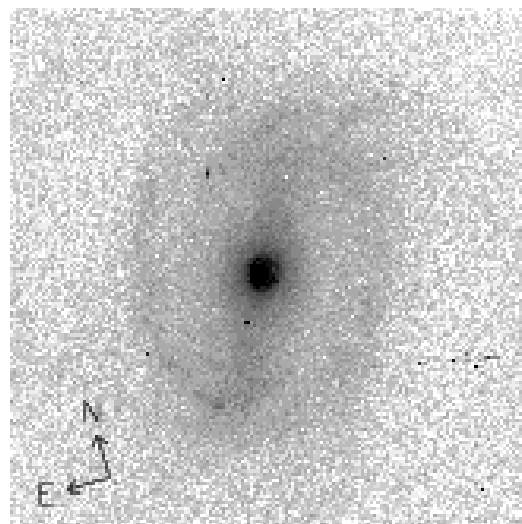
^aReferences for FWHM – A96: Acosta-Pulido, et al. 1996, C86: Crenshaw 1986, G82: Ghigo, et al. 1982, G91: Gregory, Tiftt, & Cocke 1991, H86: Halpern & Filippenko 1986, H97 Ho et al. 1997, K83: Kollatschny & Fricke 1983, K00: Kollatschny, Bischoff, & Dietrich 2000, K91: Kriss et al. 1991, M03: Marziani et al. 2003, O77: Osterbrock 1977, O81: Osterbrock 1981, O82: Osterbrock & Shuder 1982, R00: Rodriguez-Ardila, Pastoriza, & Donzelli 2000, S90: Stirpe 1990, V01: Véron-Cetty, Véron, & Gonçalves 2001, W92: Winkler 1992

^bObserved with the F814W filter.

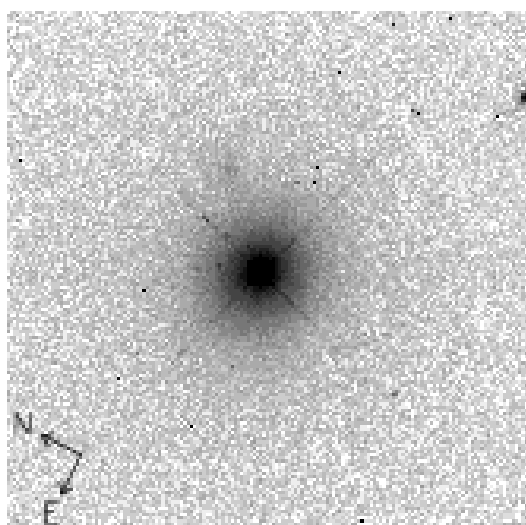
^cObserved with the F547M filter.



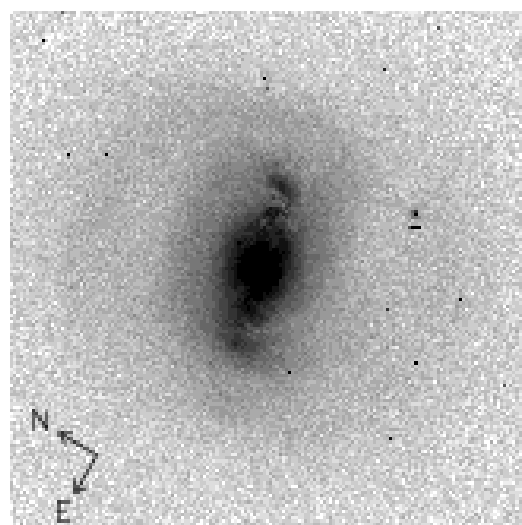
MCG 6-26-12 (20.9 x 20.9 kpc)



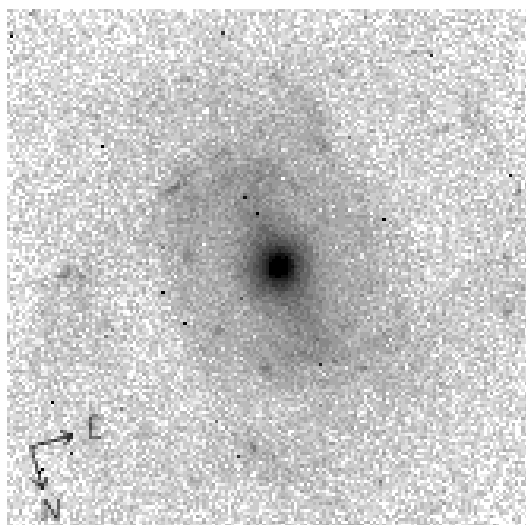
Mrk 42 (15.7 x 15.7 kpc)



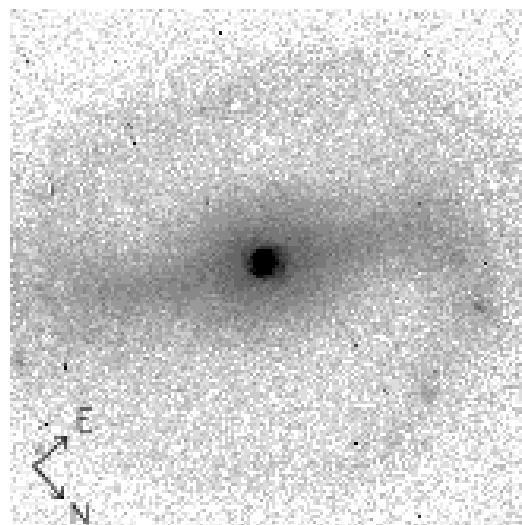
Mrk 335 (16.3 x 16.3 kpc)



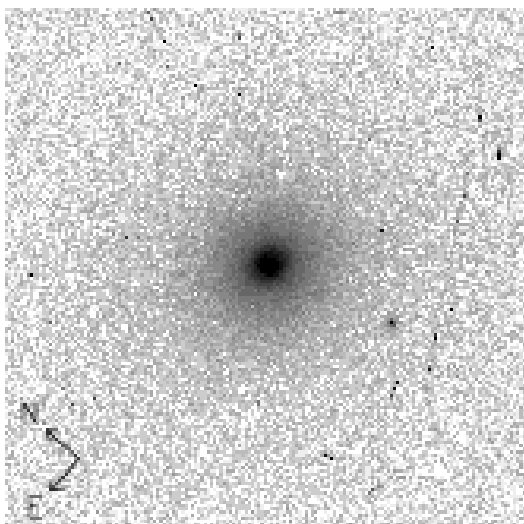
Mrk 359 (11.1 x 11.1 kpc)



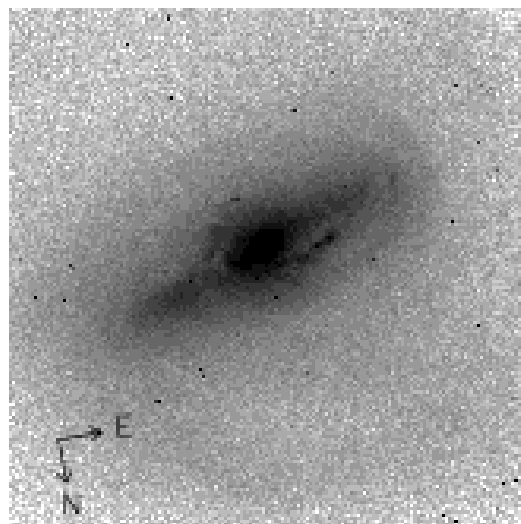
Mrk 382 (22.2 x 22.2 kpc)



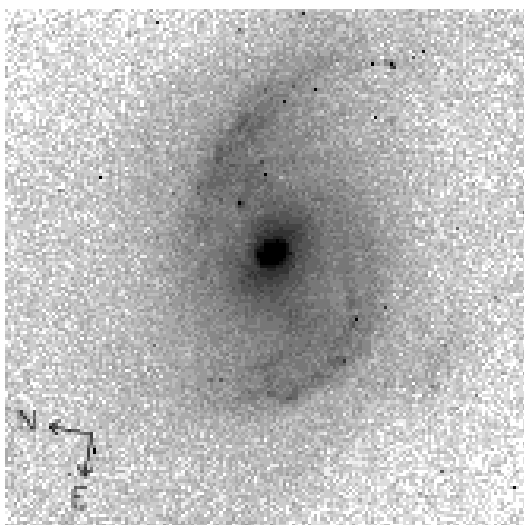
Mrk 493 (20.2 x 20.2 kpc)



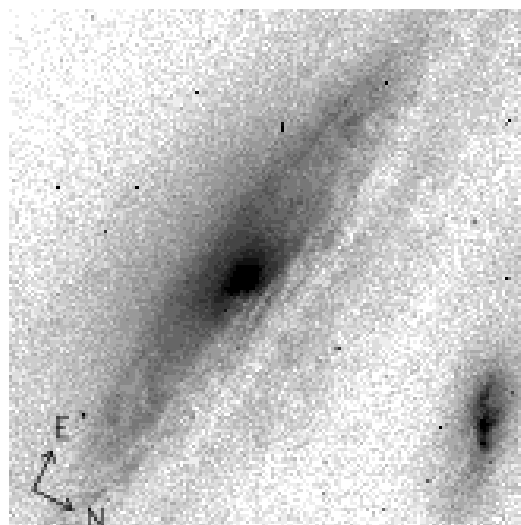
Mrk 699 (22.2 x 22.2 kpc)



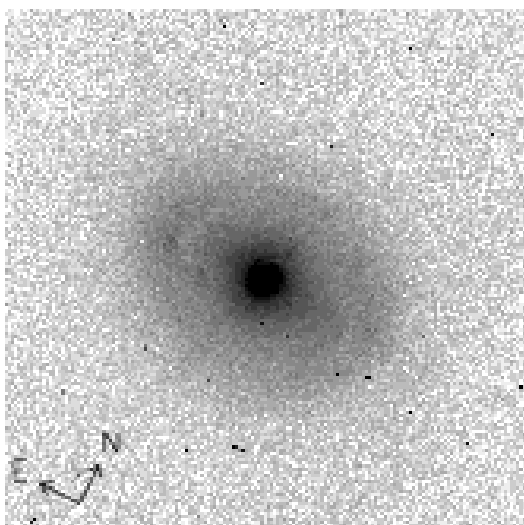
Mrk 766 (7.8 x 7.8 kpc)



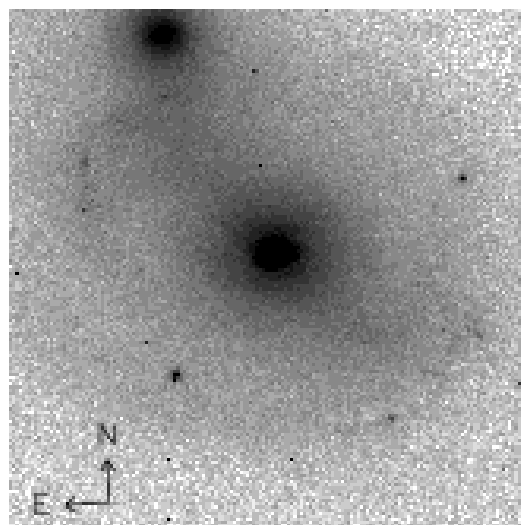
Mrk 896 (17.6 x 17.6 kpc)



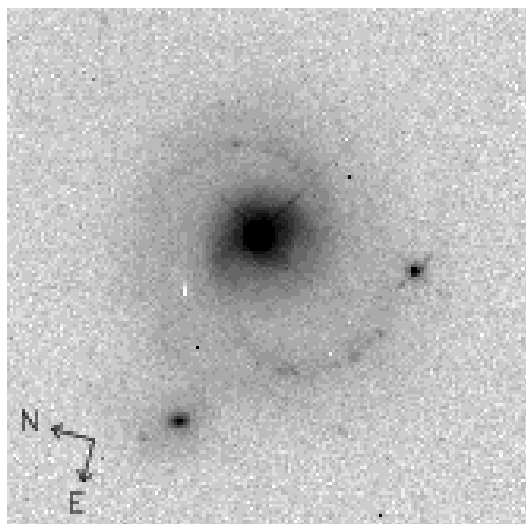
Mrk 1044 (10.4 x 10.4 kpc)



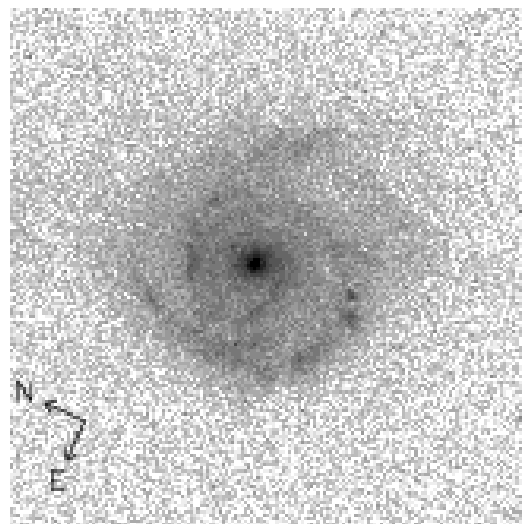
NGC 4051 (1.3 x 1.3 kpc)



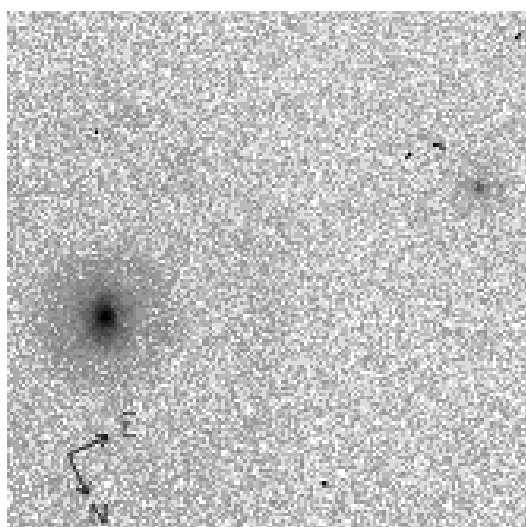
NGC 4748 (9.1 x 9.1 kpc)



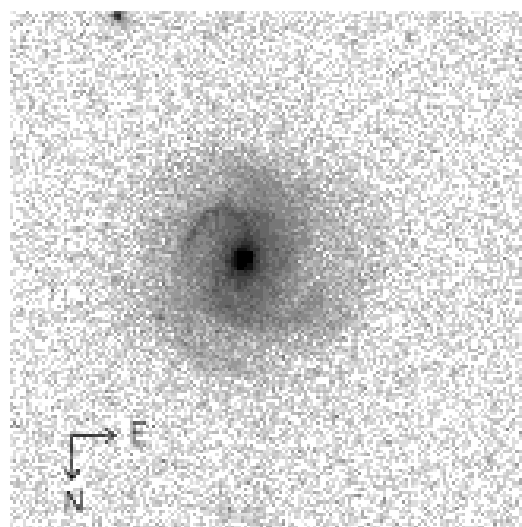
I Zw 1 (21.6 x 21.6 kpc)



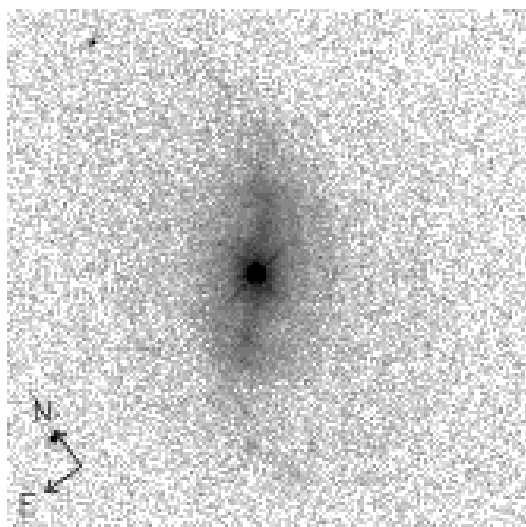
MS 01442-0055 (28.3 x 28.3 kpc)



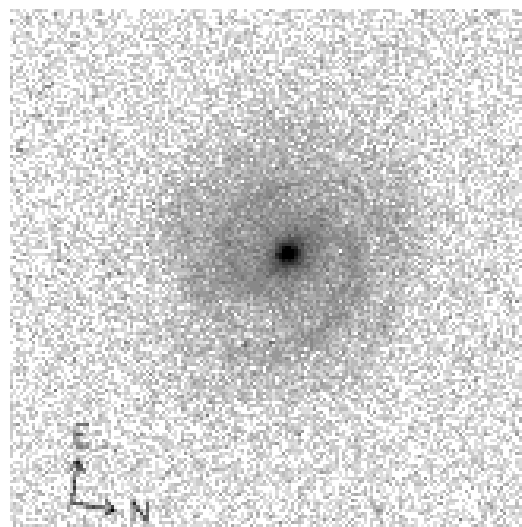
Mrk 705 (9.9 x 9.9 kpc)



MS 12170+0700 (28.3 x 28.3 kpc)



MS 15198-2107 (29.7 x 29.7 kpc)



MS 22102+1827 (27.9 x 27.9 kpc)

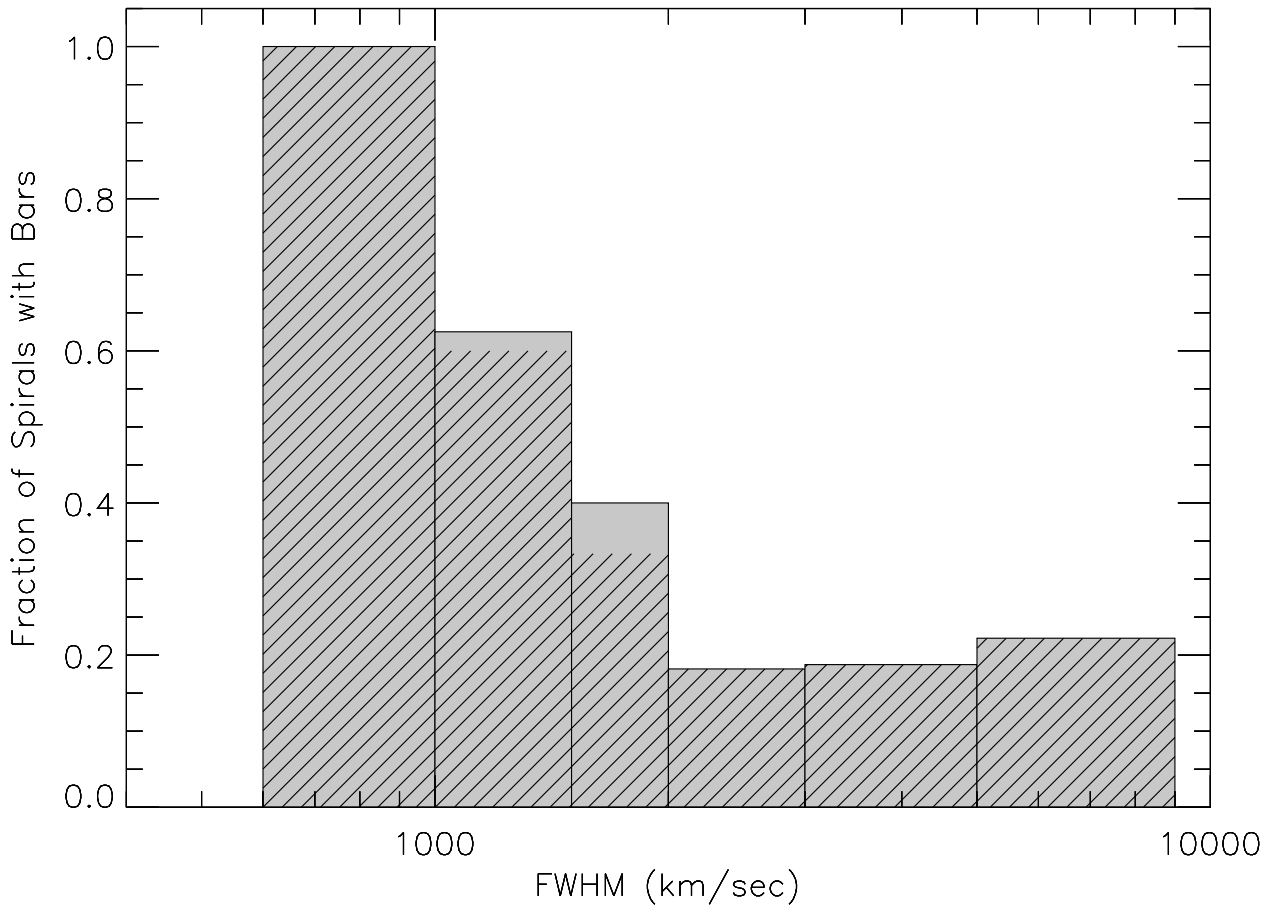


Fig. 3.